Density Functional Theory Study of the Thermodynamic and Raman Vibrational Properties of γ-UO_3 Polymorph

Francisco Colmenero[a], *Laura. J. Bonales*[b], *Joaquín Cobos*[b] *and Vicente Timón*[a*]

[a] Instituto de Estructura de la Materia (CSIC). C/ Serrano, 113. 28006 – Madrid, Spain.

[b] Centro de Investigaciones Energéticas, Medioambientales y Tecnológicas (CIEMAT). Avda/ Complutense, 40. 28040 – Madrid, Spain.

*E-mail: vicente.timon@csic.es

ABSTRACT

Gamma uranium trioxide, γ-UO_3, is one of the most important polymorphs in uranium trioxide system which is common throughout the *nuclear fuel cycle* and used industrially in the reprocessing of nuclear fuel and uranium enrichment. In this work, a detailed theoretical solid-state density functional theory study of this material was carried out. The computed lattice parameters, bond lengths, bond angles and X-Ray powder pattern were found in very good agreement with their experimental counterparts determined by X-Ray diffraction. The equation of state of γ-UO_3 was obtained and, therefore, the values of the bulk modulus and its derivatives, for which there are not experimental data to compare with, were predicted. The computed bulk modulus differs from that of a previous density functional theory calculation by only 4.4%. The thermodynamic properties of this material, including heat capacity, entropy, enthalpy, free energy and Debye temperature were also determined as a function of temperature in the range 0-1000 K. The computed low- and high-temperature thermodynamic functions are in excellent agreement with the experimental ones determined from calorimetric measurements. At ambient temperature, the computed values of heat capacity, entropy, enthalpy and free energy differ from the experimental values by 5.3, 3.3, 3.9 and 2.6%, respectively. Finally, the Raman spectrum was determined and compared with the experimental one and was found to be in good agreement. A normal mode analysis of the theoretical spectra was carried out and used in order to resolve the uncertainty of the assignment in the observed Raman bands. The assignment permits to attribute the different bands to vibrations localized in the different distorted octahedra associated to the two non-equivalent uranium atom types present in the structure of γ-UO_3.

KEYWORDS

γ-UO_3, DFT, Equation of state, Thermodynamics, Raman spectroscopy

I. INTRODUCTION

Uranium trioxide, UO_3, also called uranyl oxide, is the oxide of hexavalent uranium and is a poisonous radioactive yellow-orange material. The UO_3 system is an extraordinarily important and complex polymorphic system which has not been fully characterized, even though the species involved are common throughout the *nuclear fuel cycle*.[1-6] Uranium trioxide is used industrially in the reprocessing of nuclear fuel (PUREX/UO_3 method[3]) and uranium enrichment.[4] Modern uranium refineries produce uranium trioxide of a very high degree of purity.[5]

Since production processes of uranium trioxide result in mixtures of the different polymorphic phases and small changes in the conditions of these processes affect the phase genesis giving rise to differences in the final products, the study of UO_3 system components is very useful in order to understand the process history. Sweet *et al.*[1-2] studied this system through the combined application of traditional (X-Ray diffraction) and a variety of optical techniques. These authors developed Raman and fluorescence spectroscopic libraries for pure and mixed polymorphic forms of UO_3 in addition to the common hydrolysis products of UO_3.

Uranium trioxide exists in at least seven crystalline forms plus an amorphous form.[7-8] The α[9-13] and γ[14-18,13] forms have been studied crystallographically, the γ modification being the best well defined by experimental data.[18] The structures of the β, δ, η and ε[19-21,8] polymorphs are less well established. The last crystalline form is a high-pressure modification reported by Siegel and Hoekstra.[8]

The research on the field of thermodynamics of nuclear materials is strongly stimulated by the demands of the nuclear technology. Fundamental thermodynamic data are the indispensable basis for a dynamic modelling of the chemical behavior of nuclear materials.[22-24] The thermodynamic modelling of the O–U system is of first importance in the development of a nuclear thermodynamic

database.[25-26] The enormous relevance of the thermodynamic information of uranium containing materials is reflected by the large number of recent experimental works on this topic culminating in large reviews and updates of thermodynamic properties of uranium bearing species[27-30] and other systems containing related elements.[31] While the thermodynamic information database of uranium bearing species is very advanced, there are many systems for which the corresponding data is inaccurate due to large experimental uncertainties.[32] Additionally, the range of conditions (*i.e.*, temperature and pressure) for which these properties are known is quite limited. These features point out the need of additional methods for determining these properties accurately. The thermodynamic properties of γ-UO_3 have been studied in many previous works during the last seven decades[33-39,22,25-26] and are quite well known. For this reason, it can be used as a model system to evaluate the cost and accuracy of the methods employed to determine thermodynamic properties. Present work and previous studies[40-41,24] suggest that theoretical methods, free of the difficulties associated to the handling of radioactive materials, constitute a good alternative for the determination of thermodynamic properties.

The availability of great amount of thermodynamic information of uranium containing materials contrast with the total absence of experimental data concerning the mechanical properties of these materials.[42] Theoretical methods may also be advantageous to determine these properties.[41-44] While theoretical solid state methods may be used in order to obtain these properties, the calculations required are very complex and expensive.[45-46] In this work, the equation of state of γ-UO_3 is obtained and therefore the values of the bulk modulus and its derivatives are reported.

Hoekstra and Siegel[7] have reported the infrared spectra α, β, γ, and δ polymorphs. The optically active vibrations of α form were studied by Tsuboi *et al.*[47] who observed the infrared spectra, calculated a set of force constants, and predicted the observable Raman bands. Excellent infrared

data of the UO_3 molecule isolated in an argon matrix have been reported by Gabelnick *et al.*[48]. The low frequency vibrational modes of UO_2 and UO_3 isolated in an argon matrix have been observed by Green *et al.*[49]. Density functional theory (DFT) calculations of the infrared and Raman spectra of isolated UO_3 molecule were performed by Shundalau *et al.*[50]. As noted by Armstrong *et al.*[51], the data for isolated UO_3 plus the data reported by Tsuboi *et al.*[47] for α-UO_3 should provide a starting point for the assignment of γ-UO_3 infrared and Raman spectra but, unfortunately, the integrity of UO_3 group is not maintained in the crystal and the structure of the γ form is very different from that of α form. In its structure two kinds of U atom octahedral coordination types exists, one of them being highly distorted. The interpretation of the structural data for γ-UO_3 is complicated by the fact that it seems to exist with different lattice structures at different temperatures.[18] At 293K, it is orthorhombic (*Fddd O2* space group) and since the departure from tetragonal (*$I4_1/amd$* space group) is very small, it has been described as pseudo-tetragonal. Furthermore, not all the theoretically active modes have enough intensity to be observed, and many of them considerably overlap, especially when the crystal is observed at room temperature. Therefore, the number of bands is reduced considerably.

The Raman spectrum of γ-UO_3 was observed by Armstrong *et al.*[51] and Sweet *et al.*[1-2]. A strong band was observed at 766 cm^{-1}, a medium strength band at 335 cm^{-1}, and weaker bands appear at 690, 483, 235, 103 and 51 cm^{-1}. While the strong Raman band at 766 cm^{-1} is probably a result of the stretching of the nearly linear UO_2 groups, the assignment of the remaining bands cannot be made without considerable additional data, such as single crystal polarization data and more infrared data. Due to the difficulties in the assignation of the Raman bands, quantum mechanical solid state calculations of γ-UO_3 were carried out. This first principles treatment should resolve all the uncertainties involved in the spectroscopic Raman study of this polymorphic form of UO_3

including a rigorous assignation of all spectral bands. In fact, present study allowed assigning the Raman bands to vibrations localized in the distorted octahedra associated to two different uranium atom types present in the structure of γ-UO_3.

Using density functional theory, He *et al.*[52] calculated the band gaps of α-, δ-, and γ-UO_3. Geng *et al.*[53] also calculated the band gap of δ-UO_3. Pickard *et al.*[54] also performed DFT calculations on α-, δ-, and η-UO_3, reporting lattice parameters and atomic coordinates. Finally, Brincat *et al.*[44] performed DFT computations of the structural and mechanical properties of UO_3 polymorphs α-, β-, γ-, δ- and η-UO_3 and studied their thermodynamic stability. In the works of He *et al.*[52] and Brincat *et al.*[44] the γ-UO_3 polymorph was considered. In both studies, high-quality DFT calculations were performed. However, the calculated structure by He *et al.*[52] has tetragonal symmetry (*$I4_1$* space group) and they reported only a very small amount of results concerning γ-UO_3. In the study of Brincat *et al.*[44] the orthorhombic *Fddd* structure was studied and detailed structural and mechanical results were given. These authors employed the DFT+U methodology[45] (GGA-PBE functional improved by means of the addition of Hubbard correction). However, the unit cell volume resulting from these calculations appears to overestimate the experimental value by nearly 9%. Their computed bulk modulus from the elasticity tensor, differs from the value computed from the equation of state in this work by only 4.4%. While these authors studied the thermodynamic stability of UO_3 polymorphs with respect to pressure[44], the thermodynamic functions and vibrational properties of γ-UO_3 polymorph were not determined.

This paper is organized as follows. In Section 2, the methods used in this work are described. In Section 3, the main results of this paper are reported and discussed. The structure of γ-UO_3 is studied and the calculated lattice parameters, bond lengths, bond angles, and X-ray powder pattern are given and compared with the corresponding experimental data. The equation of state and

thermodynamic properties of γ-UO_3 are also reported. The theoretical Raman spectrum of this system is provided and the assignment of the main bands in the spectrum is carried out. Finally, the conclusions of this work are given in Section 4.

II. METHODS

The unit cell of γ-UO_3 has been modeled using the CASTEP code,[55] a module of the Materials Studio package.[56] The generalized gradient approximation (GGA) with PBESOL functional[57-58] was used. Geometry optimization was carried out using the Broyden–Fletcher–Goldfarb–Shanno optimization scheme[59-60] with a convergence threshold on atomic forces of 0.01 eV/Å. The kinetic energy cutoff employed was 1000 eV and the corresponding k-point mesh[61] adopted was 3 x 3 x 1 (4 K points). They were selected by performing calculations of increasing complexity. The above calculation parameters gave well converged structures and were considered sufficient to determine the final material properties.

The norm-conserving relativistic pseudopotential[62] for uranium atom employed in the computations was generated in our previous work[63] and successfully used in other publications.[64,41,43] The pseudopotential for O atom in the unit cell of γ-UO_3 was a standard norm-conserving pseudopotential given in CASTEP code (00PBE-OP type).

Bulk modulus and its pressure derivatives were calculated by fitting the lattice volumes and pressures to an equation of state. In the present study, the lattice volumes around the equilibrium were computed by optimizing the structure at several different pressures between -1.0 and 12.0 GPa, where negative pressure values mean traction or tension. The results were then fitted to a fourth-order Birch-Murnaghan[65] equation of state using the computed volume at 0 GPa as V_0 using EOSFIT 5.2 code.[66]

The phonon spectrum at the different points of Brillouin zone can also be determined by DFPT as second order derivatives of the total energy.[67] Phonon dispersion curves and density of states were calculated and, from them, several important thermodynamic quantities in the quasi-harmonic approximation, such as free energies, enthalpies, entropies, specific heats and Debye temperatures were evaluated.[67-68]

The linear response density functional perturbation theory[67,69-70] (DFPT) implemented in the CASTEP code was used to obtain the vibrational properties, where phonon frequencies at the gamma point of the Brillouin zone were computed using atomic displacement perturbations. Raman intensities are third-order derivatives of total energy with respect to vibrational mode (atomic position) and laser field (electric field, twice). These are calculated in CASTEP[71] by using a combination of perturbation theory (second derivative with respect to field) and finite differences (third derivative with respect to atomic displacement). The frequencies presented in this work have not been scaled to correct for anharmonicity and remaining errors of the theoretical treatment employed, such as incomplete treatment of electron correlation and basis set truncation.[72]

III. RESULTS AND DISCUSSION

III.1. Structure

As it can be seen in Fig. 1, uranium atoms in γ-UO_3 (of types U1 and U2) display octahedral coordination. The octahedra, especially those surrounding U1 (see Fig. 1.B), are very distorted. The U2 polyhedra share opposite equatorial edges (O2-O2) forming chains along *a* and *b* directions. The chains are showed in Fig. 1.A. The chains are parallel at a given *c* forming planes at different *c*'s linked with U1 polyhedra. As it can be appreciated in Fig. 1.B, the chains are directed alternatively along *a* and *b* when *c* decreases. U1 polyhedra share two vertices of two

contiguous U2 polyhedra (O1 axial vertices) along a chain at a given plane and two vertices of U2 polyhedra (O2 equatorial vertices) of two different parallel chains (see Figure 1.B) of the next plane. The optimized structure of γ-UO_3 full unit cell is displayed in Fig. 2.

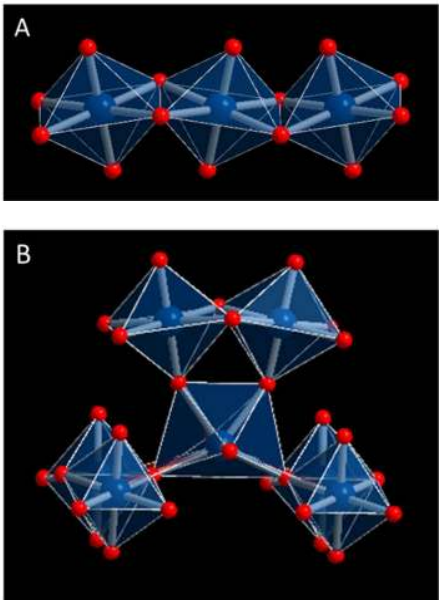

Figure 1. γ-UO_3 structure images; A) U2 polyhedra share opposite equatorial edges (O2-O2) forming chains along *a* and *b* directions; B) U2 chains are parallel at a given *c* forming planes at different *c*'s linked with U1 polyhedra. The chains are directed alternatively along *a* and *b* when *c* decreases. Color code: U-Blue, O-Red.

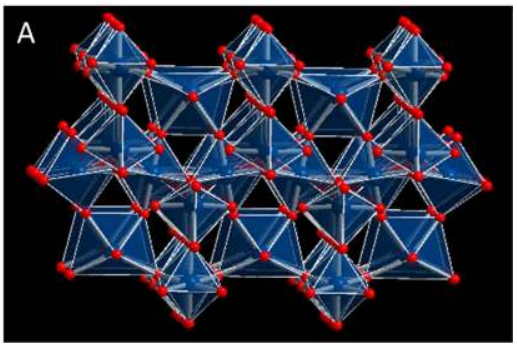

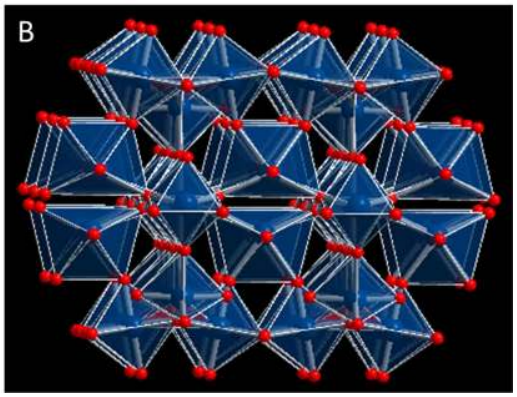

Figure 2. γ-UO_3 unit cell; A) View from [010] direction; B) View from [100] direction. Color code: U-Blue, O-Red.

The γ-UO_3 optimized lattice parameters, volume and density are compared in Table 1 with the corresponding experimental results. The DFT lattice parameters of Brincat *et al.*[44] are also given in this table. As it can be seen their calculated *c* lattice parameter overestimates the experimental value by a very large amount 0.75 Å (3.8%). Tables 2 and 3 contain the computed atomic bond distances and angles compared with the corresponding experimental values.

Table 1. γ-UO_3 lattice parameters.

Parameters	**a (Å)**	**b (Å)**	**c (Å)**	**α**	**β**	**γ**	**Vol. (Å^3)**	**Dens. (g/cm^3)**
This work	9.7137	9.7507	19.7162	90.0	90.0	90.0	1867.44	8.137
DFT[44]	9.94	9.93	20.68	90.0	90.0	90.0	(2041.2)	(7.44)
Exp.[18]	9.705	9.787	19.932	90	90	90	1893.2	8.027
Exp.[17]	9.813	9.711	19.93	90	90	90	1899.2	8.001

Table 2. γ-UO_3 bond distances (in Å). Note that in U1 polyhedra, O1 denotes the axial O atoms and O2 the equatorial ones. In U2 polyhedra O3 denotes the axial O atoms and O1, O2 the axial ones.

Bond	**Exp.[18]**	**Calc.**
U2 polyhedra		

U2-O1	1.866	1.886
U2-O2	2.258	2.189
U1 polyhedra		
U1-O3	1.793	1.794
U1-O1	2.258	2.303
U1-O2	2.360	2.315
U-U distances		
U1-U2	4.030	4.033
U1-U2’	4.054	4.081
U1-U1	4.229	4.228
U2-U2	3.446	3.441

Table 3. γ-UO_3 bond angles (in deg.). The O atom numbering convention is as in Table 2.

Bond	**Exp.**[18]	**Calc.**
U2 polyhedra		
O1-U2-O1’	180.0	180.0
O2-U2-O2’	180.0	180.0
O1-U2-O2	90.68	90.67
O1-U2-O2’	89.00	89.60
O2-U2-O2’	103.21	105.75
U1 polyhedra		
O3-U1-O3'	173.88	175.57
O1-U1-O1'	70.68	73.50
O2-U1-O2'	131.76	132.53
O3-U1-O1	88.48	88.05
O3-U1-O2	91.34	90.48
O1-U1-O2	78.79	76.98
O1-U1-O2'	149.44	150.49

The X-Ray pattern of γ-UO_3 was computed from the calculated structure by using the program REFLEX, a module of Materials Studio Package.[56] The resulting pattern is compared with the experimental one given by Sweet *el al.*[1] in Fig. 3. As can be seen, the agreement in line positions and intensities is quite satisfactory. The precise values of the main reflections (I ≥ 10%) in the X-Ray powder pattern of γ-UO_3 are given in Table A.1 of Appendix A of the Supporting Information. In this table, we compare the X-Ray powder pattern computed from the experimental[18] and computed structures[73] using CuK_α radiation (λ=1.540598 Å) and the corresponding experimental pattern of Connolly.[14] The use of spectra derived directly from the experimental and computed structures allows for a fair comparison of the results free of interferences or possible artifacts, such as the presence of sample impurities, since both are determined under the identical conditions. Nevertheless, the comparison with the experimental pattern[14] also leads to an excellent agreement.

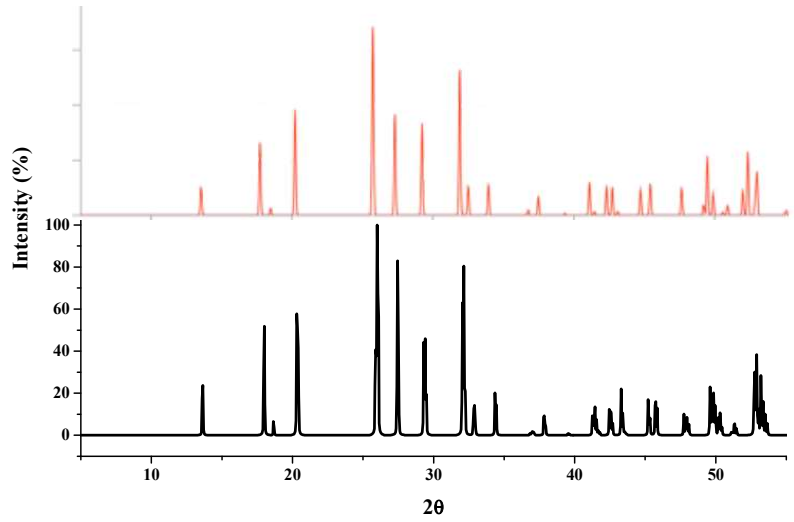

Figure 3. X-Ray powder patterns of γ-UO_3. The upper diffractogram is the experimental pattern given by Sweet *et al.*[1] and the lower one is the diffractogram computed from the calculated structure.

III.2. Equation of state

Lattice volumes around the equilibrium were calculated by optimizing the structure at seventeen different applied pressures. The results are displayed in Fig. B.1 of Appendix B of Supporting Information. The calculated data were then fitted to a fourth-order Birch-Murnaghan[65] equation of state (EOS) using the computed volume at 0 GPa (1867.4 Å^3) as V_0 using EOSFIT 5.2 code,[66]

$$P = 3\,B\,f_E\,(1+2f_E)^{\frac{5}{2}}\left[1+\frac{3}{2}(B'-4)f_E+\frac{3}{2}\left\{B\,B''+(B'-4)(B'-3)+\frac{35}{9}\right\}{f_E}^2\right]$$

In this equation,

$$f_E = \frac{1}{2}\left[\left(\frac{V_0}{V}\right)^{\frac{2}{3}}-1\right]$$

and B, B', and B'' are the bulk modulus and its first and second derivatives, respectively, at the temperature of 0 K. The values found for B, B', and B'' were B = 78.40 (±0.77) GPa, B' = 3.46 (±0.45), and B'' = –0.26 (±0.09) GPa^{-1} (χ^2 = 0.001). The value of the bulk modulus computed from the elasticity tensor by Brincat *et al.*[44], 74.9 GPa, differs from the value computed from the equation of state in this work, B = 78.40 (±0.77) GPa, by only 4.4%.

III.3. Thermodynamic properties

III.3.a. Low temperature thermodynamic properties

The calculated thermodynamic functions over the full range of temperature 0-1000 K, are given in Appendix C of the Supporting Information. Figures 4.A, 4.B, 4.C, and 4.D show the computed low temperature isobaric (zero pressure) heat capacity, entropy, enthalpy and free energy

functions, respectively, compared with the experimental data of Cordfunke and Westrum,[38] in the range of temperatures 0-300 K. The precise values of these thermodynamic functions are given in Appendix D (Table D.1) of Supporting Information. Note that all enthalpy and free energy values have been divided by the temperature to express these properties in the same units as entropy and heat capacity (J/(K·mol)).

The values of the heat capacity, entropy, enthalpy and free energy at temperatures of 100 and 298.15 K are given in Table 4. The computed thermodynamic properties are in excellent agreement with experimental data, the errors being 3.9, 1.8, 3.2 and 0.1 % at 100 K, and 5.3, 3.3, 3.9 and 2.6 % at ambient temperature, respectively. As it can be seen in Fig. 4, the calculated thermodynamic functions are very close to the experimental ones, the differences increasing slightly when the temperature increases. The absolute values of the calculated thermodynamic functions are generally smaller than the corresponding experimental values, except the free-energy values at very low temperatures.

The value obtained for the isobaric specific heat at zero pressure and 298.15 K is Cp=77.36 J/(K·mol), which may be compared with the experimental value of Cordfunke and Westrum[38] of 81.67 J/(K·mol). The agreement is very good, our value being lower than the experimental value by about 5.3%. Hemingway[22] gave a value of 84.72 J/(K·mol), which is in worst agreement with our value. The computed entropy value is S=92.96 J/(K·mol) at zero pressure and temperature of 298.15 K. Again, the agreement with the experimental value of Cordfunke and Westrum,[38] 96.11 J/(K·mol), is very good, the difference being about 3.3 %. The value of entropy given by Jones *et al.*[33] is 98.6±0.3 J/(K·mol) at 298.15 K. The calculated enthalpy value (H_T-H_0)=47.012 J/(K·mol) at zero pressure and temperature of 298.15 K, deviates from the experimental one, (H_T-H_0)=48.918

J/(K·mol), by 3.9%. Finally, the calculated free energy at 298 K, (G_T-G_0)=-45.950 J/(K·mol), is comparable to the experimental value of -47.179, the error being 2.6%.

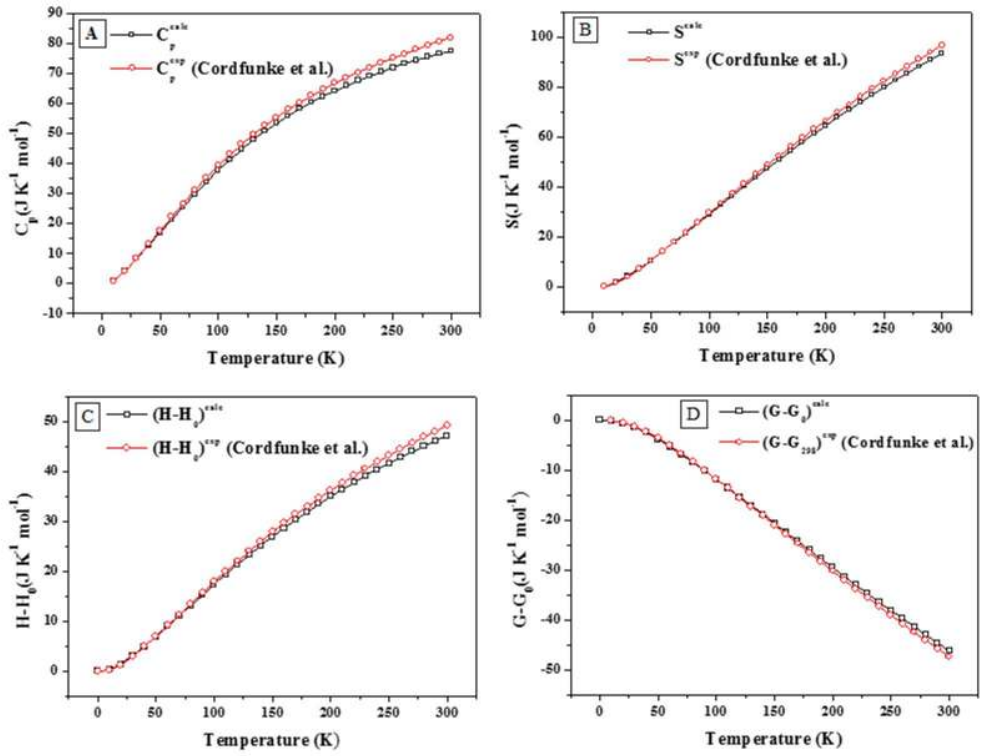

Figure 4. Comparison of calculated and experimental low-temperature thermodynamic functions: heat capacity, entropy, enthalpy and free energy (Cp, S, H-H_0, and G-G_0). The experimental data are from Cordfunke and Westrum.[38]

Table 4. Comparison of calculated and experimental thermodynamic properties at 100 and 298.15 K. All values are given in units of J/(K·mol).

Property	Exp.[38]	Calc.	Error	Error (%)
		100 K		
C_p	39.31	37.79	-1.52	-3.9
S	29.69	29.14	-0.55	-1.8
H-H_0	17.874	17.309	-0.565	-3.2
G-G_0	-11.816	-11.828	-0.012	-0.1

	298.15 K			
C_p	81.67	77.36	-4.31	-5.3
S	96.11	92.96	-3.15	-3.3
$H-H_0$	48.918	47.012	-1.906	-3.9
$G-G_0$	-47.179	-45.950	1.229	2.6

III.3.b. High temperature thermodynamic properties

Figures 5.A, 5.B, 5.C, and 5.D show the computed high-temperature isobaric (zero pressure) heat capacity, entropy, enthalpy and free energy functions, respectively, compared with the experimental data of Cordfunke and Westrum[38] and Hemingway.[22] Figure 5.E shows the calculated Debye temperature function.[41] The precise values of these properties (Cp, S, $H-H_{298}$, and $G-G_{298}$), compared with the experimental ones at temperatures of 298.15, 400, 500, 600, 700, 800, 900 and 1000 K, are given in Appendix D (Tables D.2-D.5) of the Supporting Information.

The values of the heat capacity, entropy, enthalpy and free energy at the temperature of 1000 K are summarized in Table 5. As it can be seen, even at such a high temperature, the deviations from the experimental values remain small (6.1, 3.6, 4.0, and 3.5 %, respectively). It must be noted that the value of the experimental heat capacity at 1000 K, 102.18 J/(K·mol), is above the Dulong-Petit limit of $C_p = 3nR = 99.8$ J/(K·mol). However, the calculated heat capacity at 1000 K, $C_p = 95.99$ J/(K·mol), is well below this limit. Therefore, the exact heat capacity function of γ-UO_3 should be placed between the experimental and calculated functions.

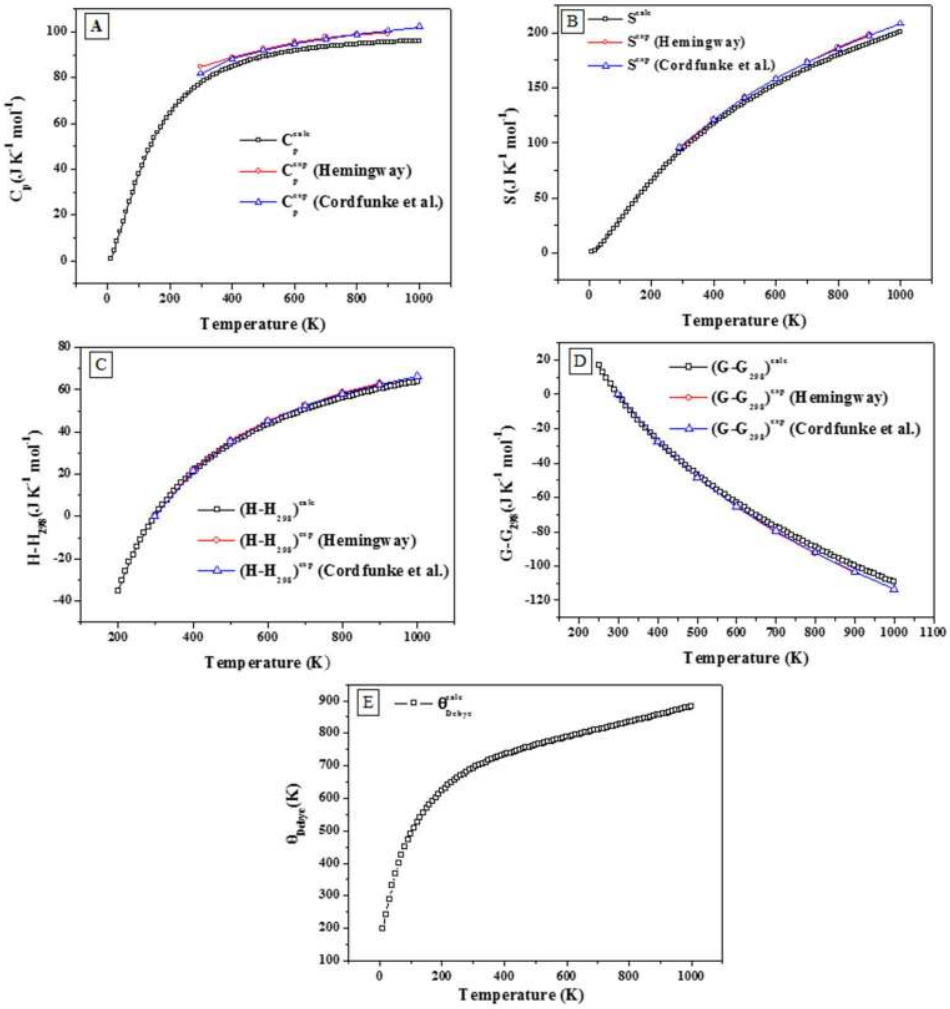

Figure 5. Comparison of calculated and experimental high-temperature thermodynamic functions: heat capacity, entropy, enthalpy, free energy and Debye temperature (Cp, S, H-H_{298}, and G-G_{298}, Θ_{Debye}). The experimental data are from Cordfunke and Westrum[38] and Hemingway.[22]

Table 5. Comparison of calculated and experimental thermodynamic properties at 1000 K. All values are given in units of J/(K·mol).

	Exp.[38]	**Calc.**	**Error**	**Error (%)**
C_p	102.18	95.99	-6.19	-6.1
S	208.45	200.85	-7.60	-3.6
H-H_{298}	66.479	63.785	-2.694	-4.0
G-G_{298}	-113.331	-109.346	-3.985	-3.5

III.4. Raman spectrum

The unit cell of γ-UO_3 of *Fddd O2* symmetry consists of 128 atoms and has 384 normal vibrations, three of which are acoustic modes. There are 42 Raman active modes whose distribution according to the irreducible representations of D_{2h} point group is $10(A_g)+10(B_{1g})+11(B_{2g})+11(B_{3g})$.

The Raman spectrum for the lowest energy *Fddd O2* structure of γ-UO_3 was computed at T=298 K, λ=532 nm, FWHM=20 cm^{-1}. The atomic motions associated to the Raman active vibrational normal modes are shown in the Supporting Information (Appendix E). Fig. 6 shows the experimental Raman spectrum of γ-UO_3 obtained by Sweet *et al.*,[1-2] together with the calculated one. A summary of the experimental and calculated spectra is shown in Table 6, as well as the assignments of the vibrational modes derived from the calculations. As can be seen in Fig. 6, the general aspect of the computed spectrum is very similar to that of the experimental spectrum. A more detailed comparison will be given below.

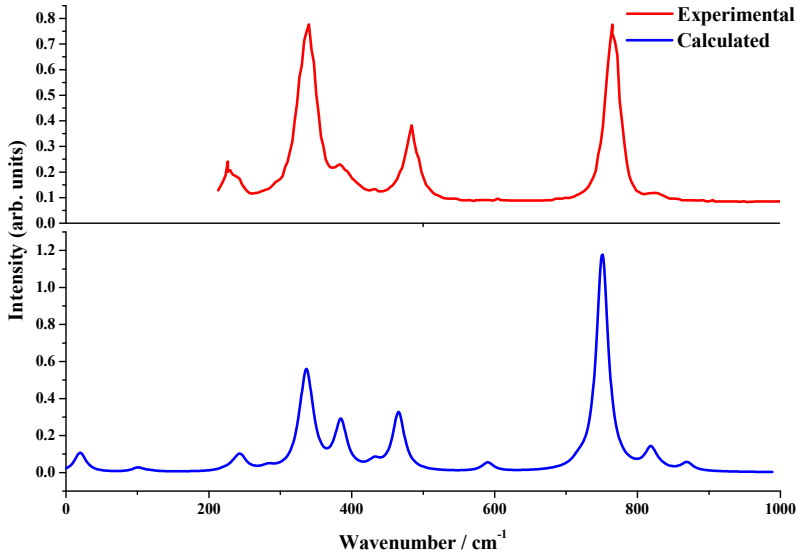

Figure 6. Calculated and experimental[1] Raman spectra of γ-UO_3.

Table 6. Calculated and experimental Raman shifts, theoretical intensities and assignations.

Calc. Raman shift (cm^{-1})	Irr. Rep. (D_{2h})	Intensity ($Å^4$)	Exp. Raman shift (cm^{-1})	Assignment
870	B_{2g}	734	-	$\nu^a(UO_2^{2+})$ for U1
869	B_{3g}	718		
818	A_g	4737	823[1]	$\nu^s(UO_2^{2+})$ for U1
752	A_g	32802	766[51], 767[1,2]	$\nu^s(UO_2^{2+})$ for U1 and U2
718	B_{2g}	351	690[51]	$\nu^s(UO_2^{2+})$ for U2
718	B_{3g}	358		
467	A_g	4440	483[51], 484[1,2]	$\rho(OUO_{eq})$ for U2+ $\delta(OUO_{eq})$ for U1
386	B_{3g}	1707	384[1]	$\rho(OUO_{eq})$ for U2+ $\nu(UO_{eq})$ for U1
385	B_{2g}	1696		
337	A_g	5339	335[51], 339[1,2]	$\rho(OUO_{eq})$ for U2+ $t(OUO_{eq})$ for U1
251	B_{2g}	244	235[51], 228[1,2]	$\rho(UO_2^{2+})$ for U2
250	A_g	158		
102	A_g	71	103[51]	T(U) for U1
28	B_{2g}	29	51[51]	$T(UO_2^{2+})$ for U1
28	B_{3g}	30		

The Raman spectrum of γ-UO_3 may be divided in three main regions covering the ranges of frequency, 900-650 cm^{-1}, 650-300 cm^{-1} and 300-0 cm^{-1}. The high frequency range is the uranyl stretching region. The band with the largest frequency observed in the experimental Raman spectrum is found at 823 cm^{-1}. In the theoretical spectrum, this band appears at 818 cm^{-1}, and it is assigned to uranyl symmetric stretching vibrations, $\nu^s(UO_2^{2+})$, where the uranium atom involved is of U1 type. The next band, observed at 767 cm^{-1}, is the most intense one in the whole Raman spectrum, the corresponding theoretical frequency being 752 cm^{-1}. It is attributed to uranyl

symmetric stretching vibrations for uranium atoms of U1 and U2 types. Finally, the band observed by Armstrong *et al.*[51] at 690 cm^{-1} corresponds to the band calculated at 718 cm^{-1}, which is associated to uranyl symmetric stretching vibrations where the uranium atom involved is of U2 type. It must be noted that an additional low intensity band at 870 cm^{-1} is observed in the theoretical spectrum, which is assigned to antisymmetric uranyl stretching vibrations, $\nu^a(UO_2^{2+})$ for uranium atoms of U1 type. Since U1 polyhedra is highly distorted, the corresponding uranyl ion is not inversion-symmetric and the corresponding band, although weak, is Raman active. The frequency of this band is very close to the value of 865 cm^{-1}, corresponding to the most intense line observed in the infrared spectrum.[7,17] This frequency is very near to that predicted from bond-length to frequency relations.[7] It must be noted that while this band was assigned by Hoekstra and Siegel[7] to uranyl symmetric stretching vibrations, our vibrational analysis shows that it should be attributed to antisymmetric stretching.

The intermediate frequency zone covers frequencies from 650 to 300 cm^{-1}. The experimental bands of this region have frequencies of 484, 384, and 339 cm^{-1} and theoretical counterparts at 467, 386 and 337 cm^{-1}, respectively. All these bands are associated to rocking vibrations, $\rho(OUO_{eq})$, for uranium atoms of U2 type, and $\delta(OUO_{eq})$, $\nu(UO_{eq})$, $t(OUO_{eq})$ vibrations for uranium atoms of U1 type, respectively, that is bending (scissoring), stretching and twisting vibrations for oxygen atoms in the equatorial plane of the U1 octahedra. As in our previous works,[64,43] with the symbol ρ we denote an antisymmetric motion of O atoms belonging to equatorial plane at opposite sides of U atom. Since the O-U-O atoms form an angle of nearly 180 degrees and the central U atom does not move during the motion, the result can be described as a planar rotation similar to a rocking vibration, usually denoted with symbol ρ (see the corresponding vibrational mode pictures in Appendix E of the Supporting Information).

In the low frequency region, 300-0 cm^{-1}, there are three main bands at frequencies 243, 103 and 51 cm^{-1} which are located in the theoretical spectrum at 251, 102 and 28 cm^{-1}, respectively. The first of these bands is assigned to rocking vibrations $\rho(UO_2^{2+})$ for uranium atoms of U2 type, that is, in this case the O atoms involved in the vibrations are not equatorial but the axial ones. The second band is attributed to a translation of the uranium U1 atom. Finally, the last band represents a translation of uranyl group, UO_2^{2+}, where the uranium atom is of U1 type. That is the last two bands are associated to translational motions of single U atoms and full uranyl UO_2^{2+} groups belonging to U1 octahedra, respectively.

IV. CONCLUSIONS

In this work, a complete study of the thermodynamic and vibrational properties of γ-UO_3 has been carried out by means of first principle calculations based on density functional theory. The great degree of agreement of computed and experimental properties found illustrates the power of theoretical methods as a predictive tool in the research of uranium containing materials.

The structural results show that there are two different types of uranium atom coordination in γ-UO_3. In both cases, the uranium atom is surrounded by six oxygen atoms displaying octahedral coordination, although the corresponding octahedra are highly distorted. The computed lattice parameters, bond lengths, bond angles and X-Ray powder pattern were found in very good agreement with their experimental counterparts determined by X-Ray diffraction.[18]

The equation of state of γ-UO_3 was obtained and, therefore, the values of the bulk modulus and its derivatives, for which there are not experimental data to compare with, were predicted. The computed bulk modulus differs from that of a previous density functional theory calculation[44] by only 4.4%.

The computed low- and high-temperature (0-300 K and 300-1000 K) thermodynamic properties, including heat capacity, entropy, enthalpy and free energy, are in excellent agreement with the experimental ones of Cordfunke and Westrum.[38] At 298.15 K, the computed values of these properties differ from the experimental values by 5.3, 3.3, 3.9 and 2.6 %, respectively. While experimental isobaric heat capacity function at 1000 K is above the Dulong-Petit limit, the computed function satisfies properly the requirement of being below the limit.

Raman spectrum of γ-UO_3 was determined by density functional perturbation theory and compared with the experimental one. Again, both spectra were found to be in very good agreement. The three main bands used to fingerprint this material,[1-2] placed at 767, 484 and 339 cm^{-1}, are very satisfactorily reproduced at 752, 467 and 337 cm^{-1}. A normal mode analysis of the theoretical spectra was carried out and used in order to resolve the uncertainty of the assignment in the observed Raman bands. The assignment permits to assign the different bands to vibrations localized in the different distorted octahedra associated to the two non-equivalent uranium atom types present in the structure of γ-UO_3.

SUPPORTING INFORMATION

This article contains supplementary information. The main reflections in the X-Ray powder pattern of γ-UO_3 are given in Appendix A. Appendix B contains a figure representing γ-UO_3 unit cell volume versus applied pressure. The calculated thermodynamic functions of γ-UO_3 (isobaric specific heat, entropy, enthalpy, free energy and Debye temperature) in the range of temperature 0-1000 K are given in a series of tables in Appendix C. The calculated and experimental high and low thermodynamic functions of γ-UO_3 are compared in Appendix D. Finally, the atomic motions associated to the Raman active vibrational normal modes are shown in Appendix E.

AUTHOR INFORMATION

Corresponding Author

*E-mail: vicente.timon@csic.es. Phone number: +34 915616800 Ext. 941120

ACKNOWLEDGEMENT

This work was supported by ENRESA in the project: Nº 079000189 "Aplicación de técnicas de caracterización en el estudio de la estabilidad del combustible nuclear irradiado en condiciones de almacenamiento" (ACESCO) and Project FIS2013-48087-C2-1-P. Supercomputer time by the CETA-CIEMAT, CTI-CSIC and CESGA centers are also acknowledged. This work has been carried out in the context of a CSIC–CIEMAT collaboration agreement: ''Caracterización experimental y teórica de fases secundarias y óxidos de uranio formados en condiciones de almacenamiento de combustible nuclear''. We also want to thank to Dr. Ana Mª Fernández for reading the document and many helpful comments.

REFERENCES

(1) Sweet, L.; Henager, C. H.; Hu, S.; Johnson, T. J.; Meier, D. E.; Peper, S. M.; Schwantes, J. M. *Investigation of Uranium Polymorphs*; Report PNNL-20951; Department of Energy under Contract DE-AC05-76RL01830, Pacific Northwest National Laboratory: Richland, WA, August 2011.

(2) Sweet, L.; Blake, T. A.; Henager, C. H.; Hu, S.; Johnson, T. J.; Meier, D. E.; Peper, S. M.; Schwantes, J. M. Investigation of the Polymorphs and Hydrolysis of Uranium Trioxide. *J. Radional. Nucl. Chem.* **2013**, *296*, 105–110.

(3) a) U.S. Department of Energy (US-DOE). *Environmental Impact Statement, Operation of PUREX and Uranium Oxide Plant Facilities*; DOE/EIS-0089D; Department of Energy: Hanford Site Richland, Washington, U.S., May (1982); b) Naylor, A.; Wilson, D. D. *Recovery of Uranium and Plutonium from Irradiated Nuclear Fuel*; Handbook of Solvent Extration. John Wiley and Sons: New York, 1983.

(4) a) International Atomic Energy Agency (IAEA). *Minimization of Waste from Uranium Purification, Enrichment and Fuel Fabrication*; IAEA-TECDOC-1115; International Atomic Energy Agency: Vienna, October (1999); Schulz, W. W. *Uranium Processing*; in Encyclopedia Britannica, https:// global.britannica.com/technology/uranium-processing (accessed April 21, 2017).

(5) Oliver, A. J.; Özberk, E. Conversion of Natural Uranium, in *Uranium for Nuclear Power: Resources, Mining and Transformation to Fuel*; I. Hore-Lacy, Ed.; Elsevier Science and Technology: Cambridge, 2006; Chapter 11; pp. 299–319.

(6) Benedict, M.; Pigford, T. H.; Levi, H. W. *Nuclear Chemical Engineering*; McGraw-Hill: New York, 1981.

(7) Hoekstra, H. R; Siegel, S. The Uranium-Oxygen System U_3O_8-UO_3. *J. Inorg. Nucl. Chem.* **1961**, *18*, 154–165.

(8) Siegel, S.; Hoekstra, H. R.; Sherry, E. The Crystal Structure of High Pressure UO_3. *Acta Crystallogr.* **1966**, *20*, 292–295.

(9) Zachariasen, W. H. Crystal Chemical Studies of the 5*f*-Series of Elements. I. New structure types. *Acta Crystallogr.* **1948**, *1*, 265–268.

(10) Loopstra, B. O.; Cordfunke, E. H. P. On the Structure of α-UO_3. *Rec. Trav. Chem.* **1966**, *85*, 135–142.

(11) Siegel, S.; Hoekstra, H. R. An Examination of the Symmetry of Alpha Uranium Trioxide, *Inorg. Nucl. Chem. Lett.* **1971**, *7*, 497–504.

(12) Greaves, C.; Fender, B. E. F. The Structure of α-UO_3 by Neutron and Electron Diffraction. *Acta Crystallogr. B* **1972**, *28*, 3609–3614.

(13) Kim, B. H.; Lee, Y. B; Prelas, M. A.; Ghosh, T.K. Thermal and X-Ray Diffraction Analysis Studies During the Decomposition of Ammonium Uranyl Nitrate. *J. Radioanal. Nucl. Chem.* **2012**, *292*, 1075–1083.

(14) Connolly, D. E. A New Interpretation of the X-Ray Diffraction Pattern of Mallinckrodt UO_3. *Acta Crystallogr.* **1959**, *12*, 949–951.

(15) De Wolff, P. M. On the Unit Cell of Mallinckrodt's UO_3. *Acta Crystallogr.* **1961**, *14*, 322–323.

(16) Engmann, R.; De Wolff, P.M. The Crystal Structure of γ-UO_3. *Acta Crystallogr.* **1963**, *16*, 993–996.

(17) Siegel, S.; Hoekstra, H. R. Bond-Lengths in γ-UO_3. *Inorg. Nucl. Chem. Lett.* **1971**, *7*, 455–459.

(18) Loopstra, B. O.; Taylor, J. C.; Waugh, A. B. Neutron Powder Profile Studies of the Gamma Uranium Trioxide Phases. *J. Solid State Chem.* **1977**, *20*, 9–19.

(19) Debets, P. C. The Structure of β-UO_3. *Acta Crystallogr.* **1966**, *21*, 589–593.

(20) Wait, E. A Cubic Form of Uranium Trioxide. *J. Inorg. Nucl. Chem.* **1955**, *1*, 309–310.

(21) Katz, J. J.; Gruen, D. M. Higher Oxides of the Actinide Elements. The Preparation of Np_3O_8. *J. Am. Chem. Soc.* **1949**, *71*, 2106–2112.

(22) Hemingway, B. S. *Thermodynamic Properties of Selected Uranium Compounds and Aqueous Species at 298.15 K and 1 Bar and at Higher Temperatures - Preliminary Models for the Origin of Coffinite Deposits*; USGS Open-File Report 82–619: 1982.

(23) Navrotsky, A.; Shvareva, T. Y.; Guo, X.; Rock, P. A. *Chapter 4: Thermodynamics of Uranium Minerals and Related Materials*; Mineralogical Association of Canada Short Course 43: Winnipeg, MB, May 2013.

(24) Sassani, D. C.; Jové-Colón, C. F.; Weck, P. F.; Jerden, J. L.; Frey, K. E.; Cruse, T.; Ebert, W. L.; Buck, E. C.; Wittman, R. S. *Used Fuel Degradation: Experimental and Modeling Report, Fuel Cycle Research and Development Report FCRD-UFD-2013-000404*; Sandia National Laboratories: Albuquerque, New Mexico, October 17, 2013.

(25) Chevalier, P.-Y.; Fischer, E.; Cheynet, B. Progress in the Thermodynamic Modelling of the O–U Binary System. *J. Nucl. Mat.* **2002**, *303*, 1–28.

(26) Konings, R. J. M.; Benes O.; A. Kovacs; Manara, D.; Gorokhov, D. S.; Iorish, V. S.; Yungman, V.; Shenyavskaya, E.; Osina, E. The Thermodynamic Properties of the f-Elements and their Compounds. Part 2. The Lanthanide and Actinide Oxides. *J. Phys. Chem. Ref. Data* **2014**, *43*, 013101.

(27) Wanner, H.; Forest, I., Eds. *Chemical Thermodynamics of Uranium*; Elsevier Science Publishers B.V.: Amsterdam, North-Holland, 1992.

(28) Murphy, W. M.; Pabalan, R. T. *Review of Empirical Thermodynamic Data for Uranyl Silicate Minerals and Experimental Plan*; Nuclear Regulatory Commission Contract NRC-02-93-005; Center for Nuclear Waste Regulatory Analyses: San Antonio, Texas, June 1995.

(29) Grenthe, I; Fuger, J.; Konings, R. J. M.; Lemire, R. J.; Muller, A. B.; Nguyen-Trung, C.; Wanner, H. *Chemical Thermodynamics of Uranium*; Nuclear Energy Agency Organisation for Economic Co-Operation and Development, OECD: Issy-les-Moulineaux, France, 2004.

(30) Shvareva, T. Y.; Fein, J. B.; Navrotsky, A. Thermodynamic Properties of Uranyl Minerals: Constraints from Calorimetry and Solubility Measurements. *Ind. Eng. Chem. Res.* **2012**, *51*, 607–613.

(31) Guillaumont, N. Y. R.; Fanghänel, T.; Neck, V.; Fuger, J.; Palmer, D. A.; Grenthe, I.; Rand, M. H. *Update on the Chemical Thermodynamics of Uranium, Neptunium, Plutonium, Americium, and Technetium*; Mompean, F. J., Illemassene, M., Domenech-Orti, C., Ben Said, K., Eds.; OECD Nuclear Energy Agency, Data Bank: Issy-les-Moulineaux, France, 2003.

(32) Langmuir, D. *Aqueous Environmental Geochemistry*; Prentice-Hall: New Jersey, 1997; pp 486–557.

(33) Moore, G. E.; Kelley, K. K. High-Temperature Heat Contents of Uranium, Uranium Dioxide and Uranium Trioxide. *J. Am. Chem. Soc.* **1947**, *69*, 2105–2107.

(34) Jones, W. M.; Gordon, J.; Long, E. A. The Heat Capacities of Uranium, Uranium Trioxide, and Uranium Dioxide from 15°K to 300°K. *J. Chem. Phys.* **1952**, *20*, 695–699.

(35) Cordfunke, E. H. P.; Aling, P. System UO_3+U_3O_8: Dissociation Pressure of γ-UO_3. *Trans. Faraday Soc.* **1965**, *61*, 50–53.

(36) Westrum, E. F. Recent Developments in the Chemical Thermodynamics of the Uranium Chalcogenides, in: *Thermodynamics, Vol. 2, Proc. Symp. held 22-27 July, 1965, in Vienna*, International Atomic Energy Agency: Vienna, 1966.

(37) Pankratz, L. B. Thermodynamic Properties of Elements and Oxides. *US Bur. Min. Bull.* **1982**, *672*, 509 pp.

(38) Cordfunke, E. H. P., Westrum, E. F. The Thermodynamic Properties of β-UO3 and γ-UO_3. *Thermochim. Acta* **1988**, *124*, 285–296.

(39) Gueneau, C.; Baichi, M.; Labroche, D.; Chatillon, C.; Sundman, B. Thermodynamic Assessment of the Uranium–Oxygen System. *J. Nucl. Mater.* **2002**, *304*, 161–175.

(40) a) Weck, P. F.; Kim, E. Layered Uranium(VI) Hydroxides: Structural and Thermodynamic Properties of Dehydrated Schoepite α-$UO_2(OH)_2$. *Dalton Trans.* **2014**, *43*, 17191–17199; b) Weck, P. F.; Kim, E. Uncloaking the Thermodynamics of the Studtite to Metastudtite Shear-Induced Transformation. *J. Phys. Chem. C* **2016**, *120*, 16553–16560.

(41) Colmenero, F.; Bonales, L. J.; Cobos, J., Timón, V. Thermodynamic and Mechanical Properties of Rutherfordine Mineral Based on Density Functional Theory. *J. Phys. Chem. C* **2017**, *121*, 5994–6001.

(42) Weck, P. F.; Kim, E.; Buck, E. C. On the Mechanical Stability of Uranyl Peroxide Hydrates: Implications for Nuclear Fuel Degradation. *RSC Adv.* **2015**, *5*, 79090–79097.

(43) Colmenero, F.; Bonales, L. J.; Cobos, J.; Timón, V. Structural, Mechanical and Vibrational Study of Uranyl Silicate Mineral Soddyite by DFT Calculations, submitted for publication, **2017**.

(44) Brincat, N. A.; Parker, S. C.; Molinari, M., Allen, G. C.; Storr, M. T. Ab Initio Investigation of the UO_3 Polymorphs: Structural Properties and Thermodynamic Stability. *Inorg. Chem.* **2014**, *53*, 12253−12264.

(45) Beridze, G.; Kowalski P. M. Benchmarking the DFT+U Method for Thermochemical Calculations of Uranium Molecular Compounds and Solids. *J. Phys. Chem. A* **2014**, *118*, 11797–11810.

(46) Crocombette, J. P.; Jollet, F.; Nga, L. T.; Petit, T. Plane-Wave Pseudopotential Study of Point Defects in Uranium Dioxide. *Phys. Rev. B* **2001**, *64*, 104107.

(47) Tsuboi, B.; Terada, M.; Shimanouchi, T. Optically Active Lattice Vibrations of α-Uranium Trioxide. *J. Chem. Phys.* **1962**, *36*, 1301–1310.

(48) Gabelnick, S. D.; Reedy, G. T.; Chasanov, M. G. Infrared Spectra of Matrix-Isolated Uranium Oxide Species. II. Spectral Interpretation and Structure of UO_3. *J. Chem. Phys.* **1973**, *59*, 6397–6404.

(49) Green, D. W.; Reedy, G. T.; Gabelnik, S. D. Infrared Spectra of Matrix-Isolated Uranium Oxides. III. Low-Frequency Modes. *J. Chem. Phys.* **1980**, *73*, 4207–4216.

(50) Shundalau, M. B.; Zajogin, A. P.; Komiak, A. I.; Sokolsky, A. A.; Umreiko, D.S. A DFT Modeling of the Uranium Trioxide Vibration Spectra Characteristics. *J. Spectrosc. Dyn.* **2012**, *2*. 19.

(51) Armstrong, D. P.; Jaeabek, R. J.; Fletcher, W. H. Micro-Raman Spectroscopy of Selected Solid $U_xO_yF_z$ Compounds. *Appl. Spectrosc.* **1989**, *43*, 461–468.

(52) He, H. M.; Andersson, D. A.; Allred, D. D.; Rector, K. D. Determination of the Insulation Gap of Uranium Oxides by Spectroscopic Ellipsometry and Density Functional Theory. *J. Phys. Chem. C* **2013**, *117*, 16540−16551.

(53) Geng, H. Y.; Song, H. X.; Jin, K.; Xiang, S. K.; Wu, Q. First-Principles Study on Oxidation Effects in Uranium Oxides and High-Pressure High-Temperature Behavior of Point Defects in Uranium Dioxide. *Phys. Rev. B* **2011**, *84*, 174115−174127.

(54) Pickard, C. J.; Winkler, B.; Chen, R. K.; Payne, M. C.; Lee, M. H.; Lin, J. S.; White, J. A.; Milman, V.; Vanderbilt, D. Structural Properties of Lanthanide and Actinide Compounds within the Plane Wave Pseudopotential Approach. *Phys. Rev. Lett.* **2000**, *85*, 5122−5125.

(55) Clark, S. J.; Segall, M. D.; Pickard, C. J.; Hasnip P. J.; Probert, M. I. J.; Refson, K.; Payne, M. C. First Principles Methods Using CASTEP. *Z. Kristallogr.* **2005**, *220*, 567–570

(56) MaterialsStudio, http://accelrys.com/products/materials-studio (accessed Jan 20, 2017).

(57) Perdew, J. P.; Burke, K.; Ernzerhof, M. Generalized Gradient Approximation Made Simple. *Phys. Rev. Lett.* **1996**, *77*, 3865–3868.

(58) Perdew, J. P.; Ruzsinszky, A.; Csonka, G. I.; Vydrov, O. A.; Scuseria, G. E.; Constantin, L. A.; Zhou, X.; Burke, K. Restoring the Density-Gradient Expansion for Exchange in Solids and Surfaces. *Phys. Rev. Lett.* **2008**, *100*, 136406.

(59) Payne, M. C.; Teter, M. P.; Ailan, D. C.; Arias, A.; Joannopoulos, J. D. Iterative Minimization Techniques for *Ab Initio* Total-Energy Calculations: Molecular Dynamics and Conjugate Gradients. *Rev. Mod. Phys.* **1992**, *64*, 1045–1097.

(60) Pfrommer, B. G.; Cote, M.; Louie, S. G.; Cohen, M. L. Relaxation of Crystals with the Quasi-Newton Method. *J. Comput. Phys.* **1997**, *131*, 233–240.

(61) Monkhorst, H. J.; Pack, J. D. Special Points for Brillonin-zone Integration. *Phys. Rev. B* **1976**, *13*, 5188–5192.

(62) Troullier, N.; Martins, J. L. Efficient Pseudopotentials for Plane-Wave Calculations. *Phys. Rev. B* **1991**, *43*, 1993–2006.

(63) Bonales, L. J.; Colmenero, F.; Cobos, J.; Timón, V. Spectroscopic Raman Characterization of Rutherfordine: a Combined DFT and Experimental Study. *Phys. Chem. Chem. Phys.* **2016**, *18*, 16575–16584.

(64) Colmenero, F.; Bonales, L. J.; Cobos, J.; Timón, V. Study of the Thermal Stability of Studtite by *In Situ* Raman Spectroscopy and DFT Calculations. *Spectrochim. Acta. A* **2017**, *174*, 245–253.

(65) Birch, F. Finite Elastic Strain of Cubic Crystal. *Phys. Rev.* **1947**, *71*, 809–824.

(66) Angel, R. J. Equations of State. *Rev. Mineral. Geochem.* **2000**, *41*, 35–60. EOSFIT 5.2 software, http://www.ccp14.ac.uk/ccp/web-mirrors/ross-angel/rja/soft/.

(67) Baroni, S.; de Gironcoli, S.; Dal Corso, A. Phonons and Related Crystal Properties from Density-Functional Perturbation Theory. *Rev. Mod. Phys.* **2001**, *73*, 515–562.

(68) Lee, C.; Gonze, X. Ab Initio Calculation of the Thermodynamic Properties and Atomic Temperature Factors of SiO_2 α-Quartz and Stishovite. *Phys. Rev. B* **1995**, *51*, 8610–8613.

(69) Gonze, X.; Lee, C. Dynamical Matrices, Born Effective Charges, Dielectric Permittivity Tensors, and Interatomic Force Constants from Density-Functional Perturbation Theory. *Phys. Rev. B* **1997**, *55*, 10355–10368.

(70) Refson, K.; Tulip, P. R.; Clark, S. J. Variational Density-Functional Perturbation Pheory for Dielectrics and Lattice Dynamics. *Phys. Rev. B* **2006**, *73*, 155114.

(71) Milman, V.; Refson, K.; Clark, S. J.; Pickard, C. J.; Yates, J. R.; Gao, S. P.; Hasnip, P. J.; Probert, M. I. J.; Perlov, A.; Segall, M. D. Electron and Vibrational Spectroscopies Using DFT, Plane Waves and Pseudopotentials: CASTEP Implementation. *J. Mol. Struct. Theochem* **2010**, *954*, 22–35.

(72) Hehre, W. J.; Radom, L.; Schleyer, P. V. R.; Pople, J. A. *Ab Initio Molecular Orbital Theory*; Wiley: New York, 1986.

(73) Downs, R. T.; Bartelmehs, K. L.; Gibbs, G. V.; Boisen, M. B. Interactive Software for Calculating and Displaying X-Ray or Neutron Powder Diffractometer Patterns of Crystalline Materials. *Am. Mineral.* **1993**, *78*, 1104–1107.

Table of Contents graphic